3-D Wide-Angle Investigations in the KTB Surroundings as Part of the "Integrated Seismics Oberpfalz 1989 (ISO 89)"

H. Gebrande
M. Bopp
M. Meichelböck
P. Neurieder

3-D WIDE-ANGLE INVESTIGATIONS IN THE KTB SURROUNDINGS AS PART OF THE "INTEGRATED SEISMICS OBERPFALZ 1989 (ISO89)"

H. Gebrande, M. Bopp, M. Meichelböck u. P. Neurieder *)

SUMMARY

The high reflectivity of the upper and middle crust of the Oberpfalz, both for near vertical and wide-angle reflections, was one reason for selecting this area as site for the German Continental Deep Drilling Program KTB.

A peculiarity in the middle crust beneath the KTB site is the so-called Erbendorf-Body (EB) giving rise to extremely strong wide-angle reflections. It deserves special interest because its position right on the border between the Saxothuringian and Moldanubian zones of the Variscan fold belt, the unusual high p-wave velocities (over 7.0 km/s) in its lower part at 11 to 14 km depth, and associated dipping reflectors suggest a possible lower crustal origin of the EB. A specially designed and so far unique wide-angle 3D-survey was carried out as part of the program "Integrated Seismics Oberpfalz 89" for investigating the spatial extent, the velocity distribution and the internal structure of the EB. The first results show clearly that the EB ist not a local phenomenon beneath the DEKORP4 line, but that it exists, yet with remarkable complexities, beneath the whole covered area between the Franconian Line and the Falkenberg granite complex.

The wide-angle shots were also recorded by four 3-component geophones in the KTB pilot hole at 3195 to 3295 m depth and provided convincing evidence for s-wave splitting in the upper crust SE of the KTB location. This anisotropy effect seems to be related to the overall strike and dip of rock foliation in the zone of Erbendorf-Vohenstrauß (ZEV).

1. INTRODUCTION

It is one of the major goals of the Continental Deep Drilling Program KTB to contribute to a better understanding of the nature of seismic reflectors in the subsedimentary continental crust. The high reflectivity of the upper and middle crust at the KTB site, both in the vertical incidence as well as in the wide-angle domain (DEKORP Research Group, 1988), offers promising pre-conditions for this objective. The present report deals mainly with aspects of wide-angle reflectivity, seismic wave velocities and some fundamental observations of seismic anisotropy in the KTB surroundings.

*)Authors' address: Institut f. Allg. u. Angew. Geophysik,
Theresienstr. 41/IV,
D-8000 München 2, FRG

Except for some more general information on crustal structure of the Oberpfalz derived from large-scale seismic refraction measurements in the 1960's and early 1970's (Giese 1968, 1976; Peters 1974) most knowledge available before ISO89 originated from KTB pre-site surveys (DEKORP Research Group 1988, Gebrande et al. 1989, Schmoll et al. 1989). The most outstanding feature in the wide-angle domain is the so-called Erbendorf-body (EB), a high-velocity body at 11 to 14 km depth producing extremely strong reflections in the 40 to 60 km distance range. Detailed informations on its p-wave velocities, shape and NW-SE extent were provided by a systematic, multiply covered wide-angle survey along the DEKORP4 line in 1985.

The latest result of this survey is a wide-angle image of the Earth's crust in a NW-SE section through the KTB site (Fig. 1). It was obtained by application of the 2D isochrone-migration process on wide-angle data from the 41 to 90 km offset range (Schmidt 1990). 95 shot recordings of the contractor's 200 channel spread operated from 41 to 58 km offset and of 24 3-channel MARS stations operated by universities at 60 to 90 km offset were jointly and consistently processed to provide Fig. 1. In many respects (Moho, lower crust, SE dipping reflectors) the picture is conformable to the steep-angle migration result (Schmoll et al. 1989). In spite of the general weaker structural resolving power of wide-angle reflections, some special structures are imaged even more accentuated due to their incidence dependent reflection coefficients. This is true, e.g., for the EB, which is the conspicuous wedge-shaped body at 3.5 to 5 s two-way time (TWT) beneath the KTB site (Fig. 1). Different methods of velocity analysis and model calculations have consistently revealed p-wave velocities up to or even over 7.0 km/s in the lower part of the EB (DEKORP Research Group 1988, Gebrande et al. 1989).

These unusual properties of the EB, together with its likewise pronounced steep-angle reflectivity, have given rise to several speculations on its lithological composition and its geodynamic significance, which shall not be discussed here; in general the EB is expected to be a two-dimensional SW-NE striking structure marking the Saxothuringian/Moldanubian suture at depth (Franke 1989). On the other side, there are many indications, e.g., from older refraction lines (Gebrande et al. 1989) and from the KTB reflection lines (DEKORP Research Group 1988), that lateral heterogeneities perpendicular to the DEKORP4 line may be of similar importance like in-line heterogeneities. In principle it could even not be ruled out, from the solely one-dimensional measurements along DEKORP4, that the observed strong wide-angle reflection amplitudes of the EB may be partly due to focusing by off-line structures, and that the wide-angle image of Fig.1 may contain significant side effects.

Therefore, a consequent 3D wide-angle survey was planned and realized as part of the program "Integrated Seismics Oberpfalz 1989" devoted to a comprehensive seismic investigation of the KTB surroundings.

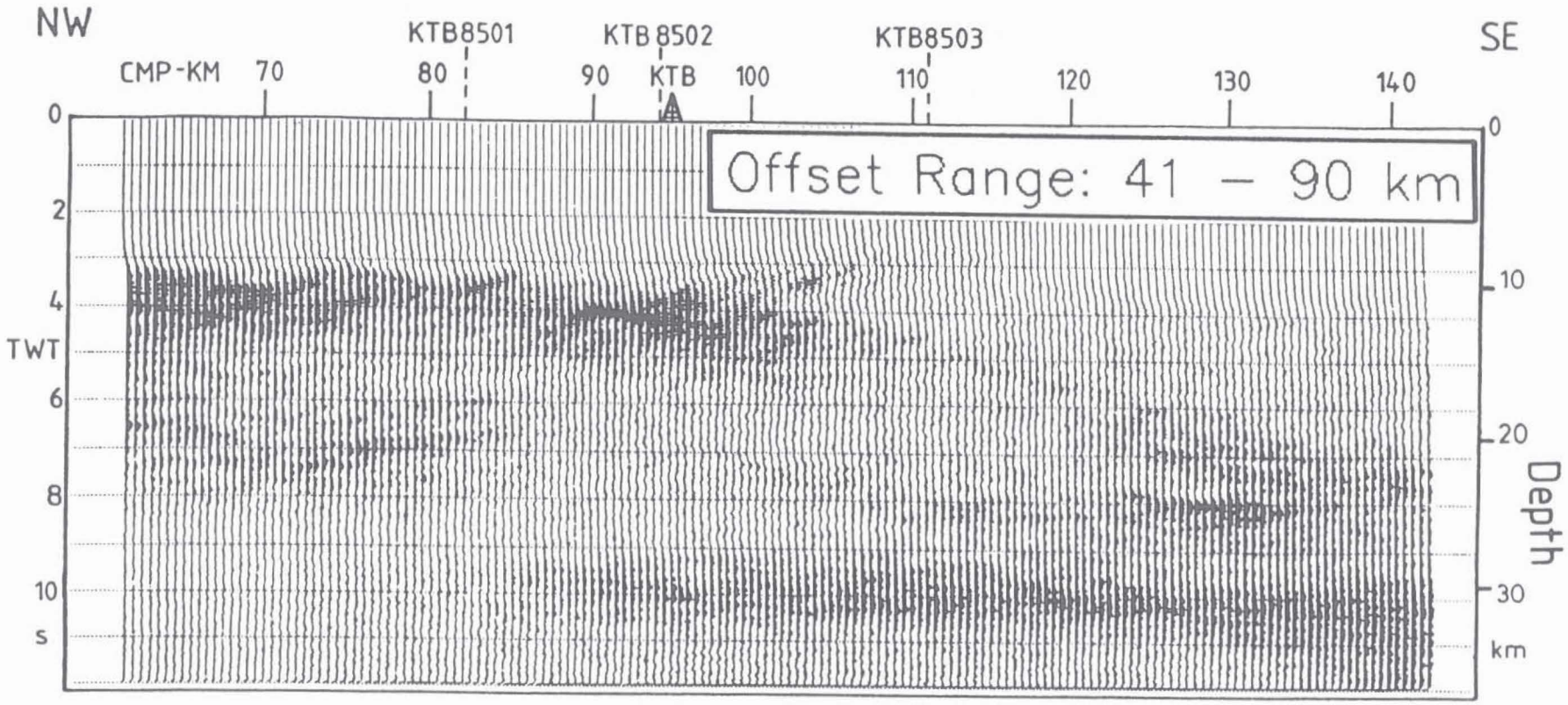

Fig. 1: Seismic image of the earth crust along a NW/SE-section through the KTB site obtained by 2D isochrone-migration of DEKORP4 wide-angle data from the 41 to 90 km offset range (after SCHMIDT, 1990). The Erbendorf-body appears as a wedge-shaped structure in the middle crust beneath the KTB location.

2. LAYOUT AND REALIZATION OF THE WIDE-ANGLE 3D-SURVEY

The basic principle of the realized 3D wide-angle survey is shown in Fig.2. The scheme consists of a linear sequence of 20 shot-points with one km spacing and a transversely oriented receiver spread. It provides single coverage in a rectangle midway between shots and receivers, the edges of which are half as long as the shot and receiver spreads, respectively. It is advisable to choose the mean shot-to-receiver offset equal to the critical distance of the reflector to be mapped, which is about 40 km for the Erbendorf body. A supplementary in-line receiver spread has been added for improved velocity resolution.

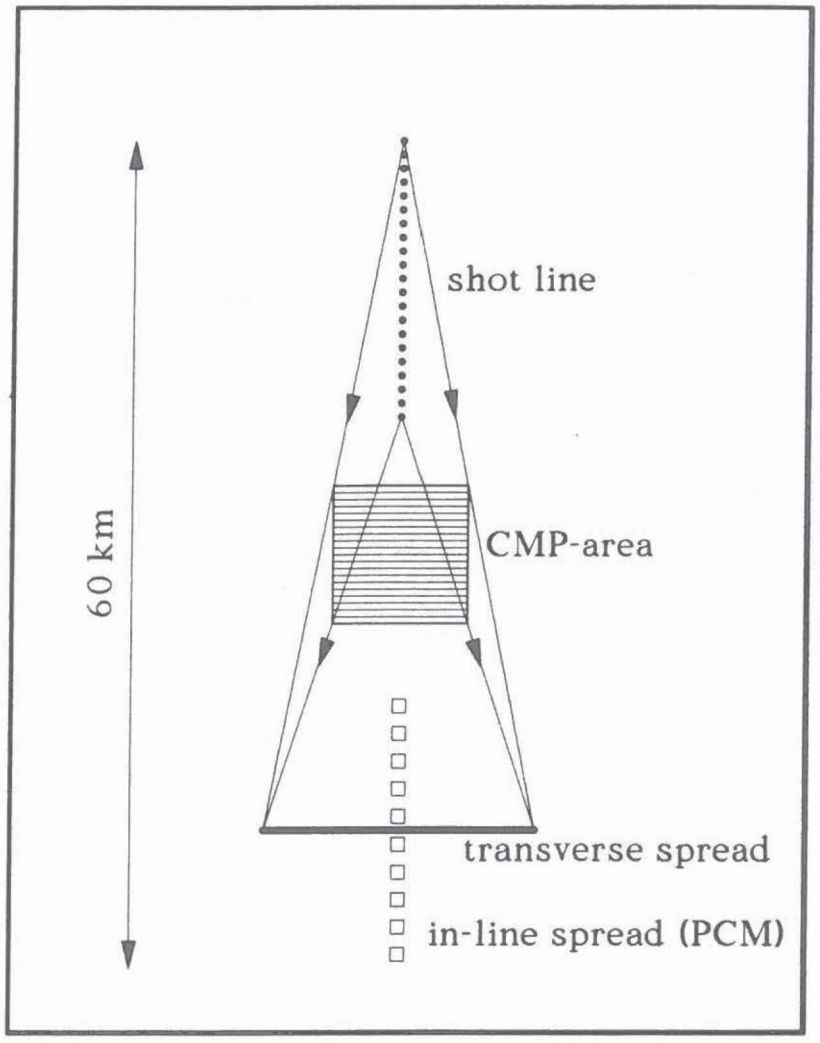

Fig. 2: Basic scheme for 3D wide-angle measurements: recording a linear shot series by a transverse oriented receiver spread of equal length at about the critical distance provides single CMP coverage in a square area in between. The supplementary in-line spread serves for improved velocity resolution.

The basic scheme of Fig.2 has been applied twice for the ISO89 wide-angle survey, once in SE-NW direction with the shot-points 101 to 120 on the former DEKORP4 line (Fig. 3) and once in SW-NE direction with shot-points 201 to 221 near to the pre-site reflection line KTB8504 (DEKORP Research Group 1988). For the latter setting shot and receiver lines have been rotated by 90° with respect to Fig. 2. Both configurations cover the same CMP rectangle with the KTB drill site in its centre.

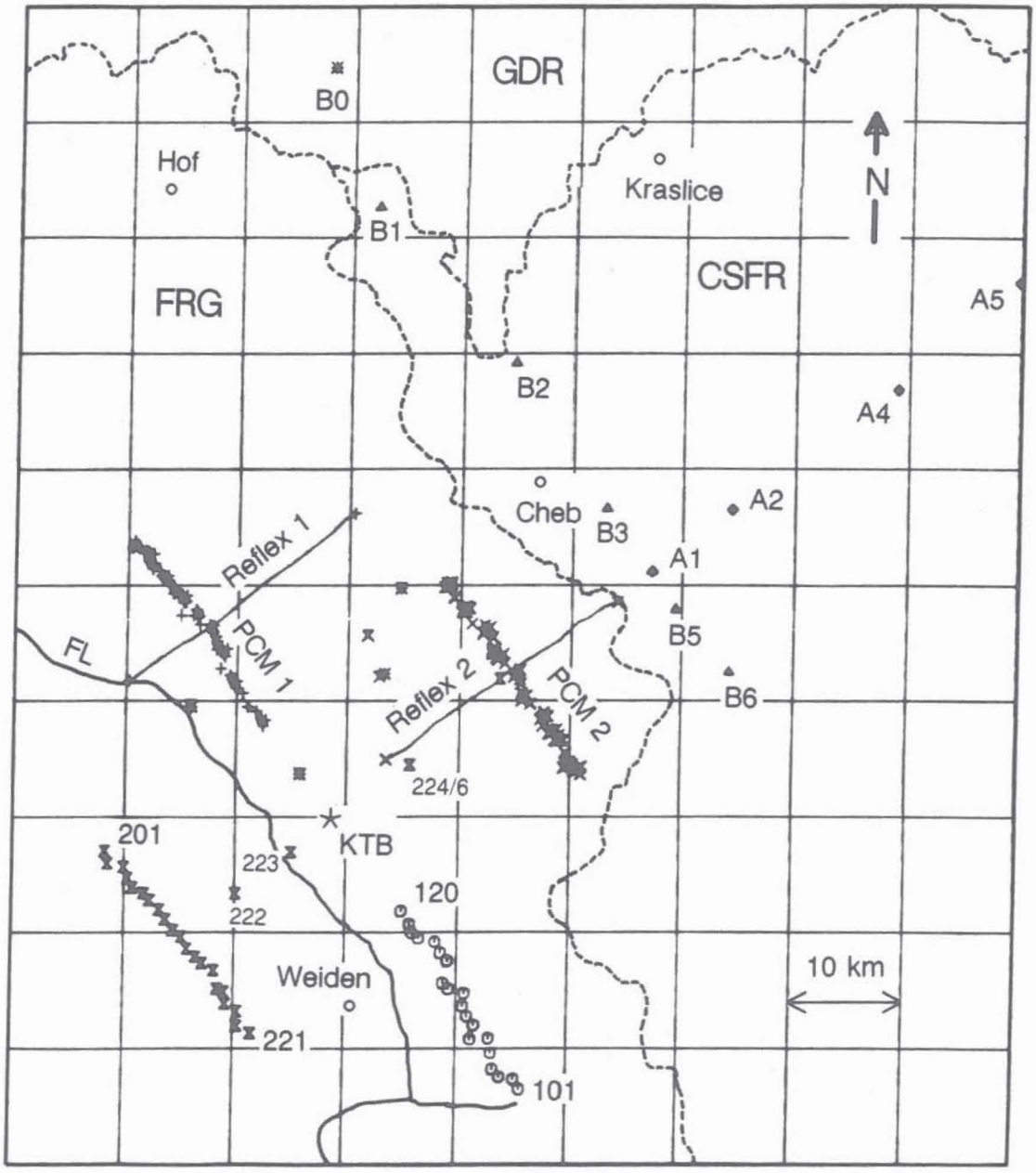

Fig. 3: Location map of ISO89 wide-angle and refraction measurements: 101-120, 201-227 shotpoints in the FRG; B0 shot in the GDR; B1-B5, A1-A5 shotpoints in the CSFR; unnumbered symbols are locations of quarry blasts. Lines Reflex1 and Reflex2 are 312-channel receiver spreads formed by 5 university and DEKORP reflection units (Table 1); perpendicular spreads PCM1 and PCM2 consist of 20 PCM stations with a total of 120 channels.

The receiver spreads normal to the shot lines, termed Reflex1 and Reflex2 in the location map (Fig. 3), were observed by means of 5 university- and DEKORP-owned reflection instruments with a total of 312 channels and 80 m receiver group spacing. The perpendicular spreads PCM1 and PCM2 were formed by 20 PCM-stations with a total of 120 channels, half of which were used for three-component recordings. Details of the instrumentation are given in Table 1.

Field work was carried out from 9th to 21th October, 1989. It was integrated in the ISO89 3D steep-angle survey and closely coordinated and synchronized with a simultaneous refraction survey by GEOFYZIKA BRNO and ZIPE POTSDAM in the adjacent territories of the CSFR and the GDR. In that way, shots fired in the Oberpfalz could also be recorded in north-western Bohemia,

Table 1: Field recording instrumentation used for the ISO89 3D wide-angle survey and effective geophone parameters

Number&Type of Recording Devices	Channels & Components	Geophon-type and Bundling	Natural Frequency [Hz]	Damping-constant	Generator Constant [Vs/cm]
1 SERCEL 338B (Muenchen)	48 vert.	2*5 SM-6/B 375Ohm	5.0	0.55	1.44
1 DFS-IV (Clausthal-Zellerfeld)	48 vert.	6 SM-6/B 375Ohm	4.6	0.55	1.88
1 DFS-V (DEKORP)	120 vert.	6 SM-6/B 375Ohm	4.6	0.95	1.65
		710hm	"	0.78	0.80
1 DFS-V (Zuerich)	48 vert.	6 SM-6/B 710hm	4.6	0.78	0.80
1 DFS-V (Karlsruhe)	48 vert.	6 SM-6/B 375Ohm	4.6	0.95	1.65
12 PCM-5800 (DEKORP,AWI)	8	6 SM-6/A	4.6	0.62	1.56
	1 3-comp. + 5 vert.	1 MUC-3D	1.0/2.0		4.00/8.00
7 PCM-5800 (Aachen,AWI)	3	1 MARK-L4A	1.0	0.62	1.00
	3-comp.	1 MUC-3D	1.0/2.0	"	4.00/8.00
1 PCM-5000 (Muenchen)	3 3-comp.	6 SM-6/A 375Ohm	4.6	0.62	1.56
1 GEOMETRICS ES-2420 (AWI)	15/3 5/1 3-comp.	2 SM-4/UHT	10.0	?	?

southern Saxony and vice-versa. Altogether 64 borehole shots (47 in the FRG, 17 in the CSFR) and 10 quarry blasts (9 in the FRG and 1 in the GDR) were observed. The contractor's recording unit for the steep-angle 3D-survey recorded the shots as well and served as master unit for radio controlled shot release and remote start of the other reflection units.

In addition all shots were also recorded in the KTB pilot hole by 3-component geophones. A geophone chain with 5 active sensors was used during shot series 101 to 120, and a single 3-component sensor during the rest of the wide-angle experiment. Details on position and orientation are given in Table 2.

3. DATA PROCESSING AND FIRST RESULTS

3.1 Preprocessing

Due to the different recording instruments used in the wide-angle survey an extensive preprocessing was required to generate a homogeneous data set. As we had decided to process the whole data volume with the DISCO software package - partially modified and extended for wide-angle applications - some extra effort was neccessary for the conversion of the non-standard PCM data into the internal Disco format. As a first step to this end, PCM data were already transformed during the experiment into a slightly modified ESSTF-format (European Standard Seismic Tape Format) and stored on computer-readable 9-track magnetic tape by means of the DEKORP PCM-playback computer, which was installed in the field headquarter; simultaneously generated analogue outputs were used for quality control.

For the straightforward input of the ESSTF data into the DISCO system an input-module "PCM" has been developed, which demultiplexes the block-multiplexed ESSTF data, converts them to DISCO format, cuts out the desired time windows from 0 to 32 s traveltime, and adds 62 shot and receiver specific header informations to each seismic trace. Finally, data were resampled to 4 ms to become compatible with multichannel reflection data.

Editing was rather time consuming and included the following steps:

- correction of polarity reversals due to non-standard polarities of some borrowed geophones,
- despiking, especially for data from the first rainy week,
- elimination of dead or strongly disturbed traces,
- zeroing of strong transient disturbances, e.g. by cars crossing cables,
- mute until about 300 ms before first arrivals,

Furthermore the data were corrected for the different geophone parameters (Table 1) and an uniform receiver response (natural frequency 4.5 Hz, damping 0.62, generator constant 100 Vs/m) was simulated by recursive simulation filtering (Seidl 1980). Finally a 6 to 40 Hz band-pass filter was applied to all data. The efficiency of these processing steps is exemplified by Fig. 4, top and centre.

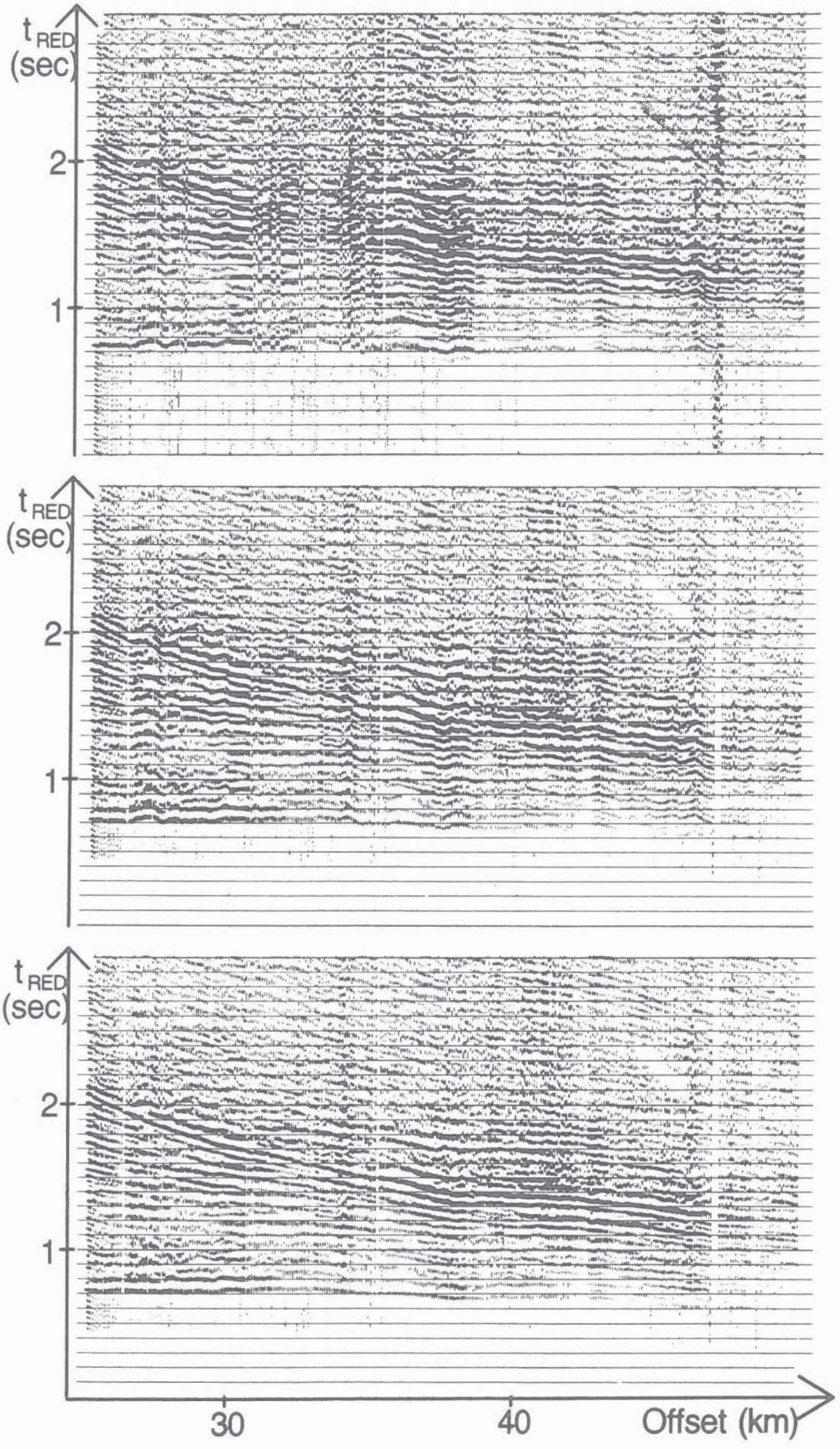
t RED
(sec)
2
1
t RED
(sec)
2
1
t RED
(sec)
2
1
30
40
Offset (km)

Fig. 4, centre, also reveals, and this is confirmed by comparative inspections of other shot records, that **static corrections** are a matter not to be ignored in wide-angle seismics. Because of missing nearby shots, however, they cannot be evaluated by standard refraction interpretation of first arrivals. Therefore we designed a two-step correlation method for the determination of short-wavelength statics and applied it, for the sake of higher resolution, to resampled data (from 4 to 1 ms). Based on 500 ms time windows around the first arrivals crosscorrelation functions of adjacent traces were stacked over 5 neighbouring shotpoints and a delay-time curve was defined along the spread by adding the individual delays of the correlation maxima picked by the interpreter. In this way 4 delay-time curves were obtained for each spread. After removal of a moving average over 5 km from each curve the remaining delay-time curves were in almost perfect agreement and there means were applied as first-order static corrections. After that, the procedure was repeated with a narrower time window of 100 ms and the resulting second-order delays were added to the first-order static corrections. The effect of applying these corrections is illustrated by comparison of Fig. 4, centre and bottom.

The general improvement of the signal-to-noise ratio from top to bottom in Fig. 4 is remarkable and will certainly increase the significance of the final results. That's why we feel it worth to do all the tedious preprocessing shortly described in this subsection.

As a typical shot record along spread Reflex2, Fig. 4 already anticipates qualitatively some main results of the present investigation:

1. The strong wide-angle reflections with 1 to 2 s reduced traveltime, which were known so far only from the NW-SE-striking DEKORP4 line and by which the Erbendorf-Body (EB) was originally defined, appear also for SW-NE propagated waves over the whole length of spread Reflex2 (Fig. 3).
2. The EB wide-angle reflections show up again with large amplitudes and apparent velocities over 7.0 km/s.

This proves that the EB is not a narrow local feature beneath the DEKORP4 line and that its large reflection amplitudes and apparent velocities are not just the results of focusing by off-line heterogeneities. This conclusions are corroborated by all other ISO89 data processed and analysed so far.

3.2 Simulated Constant-Offset (COF) and Zero-Offset Sections

For a first qualitative assessment of horizontal structural variations we use simulated constant-offset sections. They are

---

on left page:
Fig. 4: Example for signal improvement by consecutive preprocessing steps. **Top:** raw data of shot 203 recorded by spread Reflex2. **Centre:** same data after editing, mute, restitution and 6-40 Hz band-pass filtering. **Bottom:** Same data as above with static corrections applied.

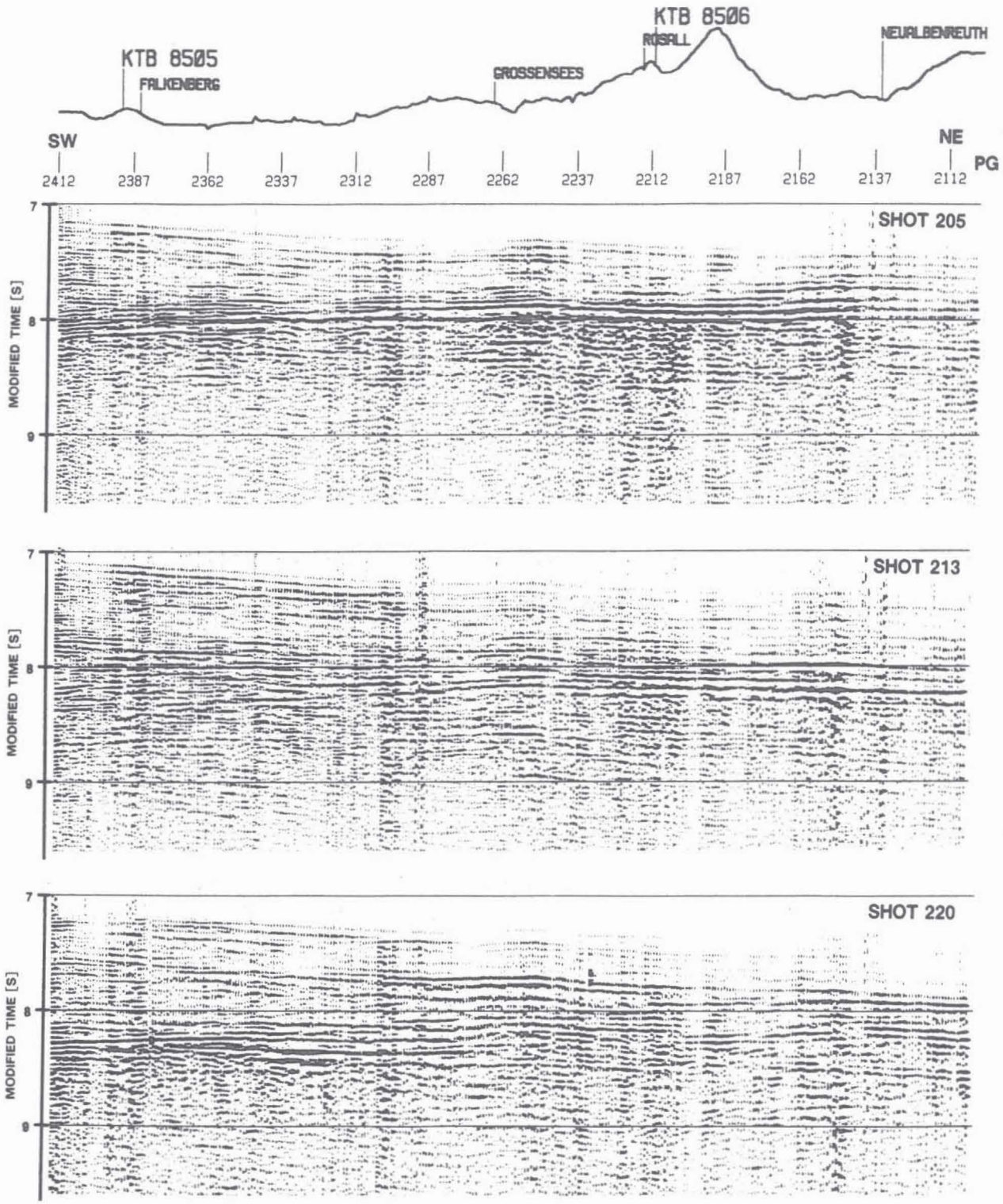

Fig. 5: Three shot records along spread Reflex2 transformed into constant offset sections (COF) by partial NMO-corrections; reference offset is 40 km. The typical wide-angle reflections from the Erbendorf-Body appear around 8 s modified time. An increase in traveltime from NW to SE and a splitting up of reflections in the SE-part (shot 220) is observed.

obtained from single-shot sections or CMP gathers by partial dynamic corrections on to a specified target offset (e.g. 40km in Fig. 5); traveltime differences due to variable shot-to-receiver offsets are thereby eliminated. We have implemented the COF-simulation process as an NMO-correction with a subsequent inverse NMO-correction on to the target offset.

In principle, any target offset would serve the purpose, but a reference value near to the mean shot-to-receiver offset has the advantages of least signal stretching and of smallest distortions in case of inaccurate NMO-velocities. For that reason 40 km has been used as COF target offset in Fig. 5. Examples are shown for three shots (205,213,220) recorded on spread Reflex2 , which are representative for the whole series of shots 201 to 221, by which the KTB surroundings were scanned in SW-NE direction. For a first overview COF simulations were performed with a constant velocity of 5.95 km/s, which - according to the DEKORP4 wide-angle results - is the best estimate of the average v_p value down to the EB.

In Fig. 5 the wide-angle reflections from the EB appear around 8 s modified time with great amplitudes and widespread continuity. The latter is very surprising in view of the generally short reflection elements observed in the crystalline crust by steep-angle seismics, e.g. on profile KTB8502 (DEKORP Research Group 1988) which partially coincides with our spread Reflex2. The EB reflections form a band which broadens from NW to SE, i.e. from shotpoint 203 towards 220. In the SE-part (shot 220) the EB seems to split up in an upper, possibly overthrusted and a lower segment, which descends to the SE.

Fig. 6 displays the same data as **simulated zero-offset (ZOF) sections.** A ZOF-section may be considered as the special case of a COF-section with total NMO corrections applied, i.e. with target offset zero. Simulated ZOF sections provide the benefit of direct comparability with steep-angle seismic results and of simple depth interpretation (with the risk of oversimplifications, however). If applied to far-offset wide-angle data, the inconvenience of serious signal distortion arises, because the NMO-corrections revoke the time-convergency of adjacent reflections with increasing offset and thereby yield considerable signal stretching at zero offset. The P_g-onsets which are most affected by stretching, and which moreover are kinematically not properly transformed by standard NMO-corrections, have therefore been suppressed in Fig. 6 by gradual muting. Structures with less than about 3.5 s zero-offset two-way time can not be resolved by our wide-angle observations starting at 25 km minimum offset.

The ZOF-sections are presented in Fig. 6 beneath a drawing of the receiver locations and their altitudes. According to the common-midpoint concept, however, the displayed reflections can be assigned to 12.5 km long, SW-NE trending midpoint lines beginning at about the Franconian Line and crossing the former DEKORP4 line 3.5 km NW, 1.0 km SE and 5.5 km SE, respectively, from the KTB location. In Fig. 6. the DEKORP4 line is situated

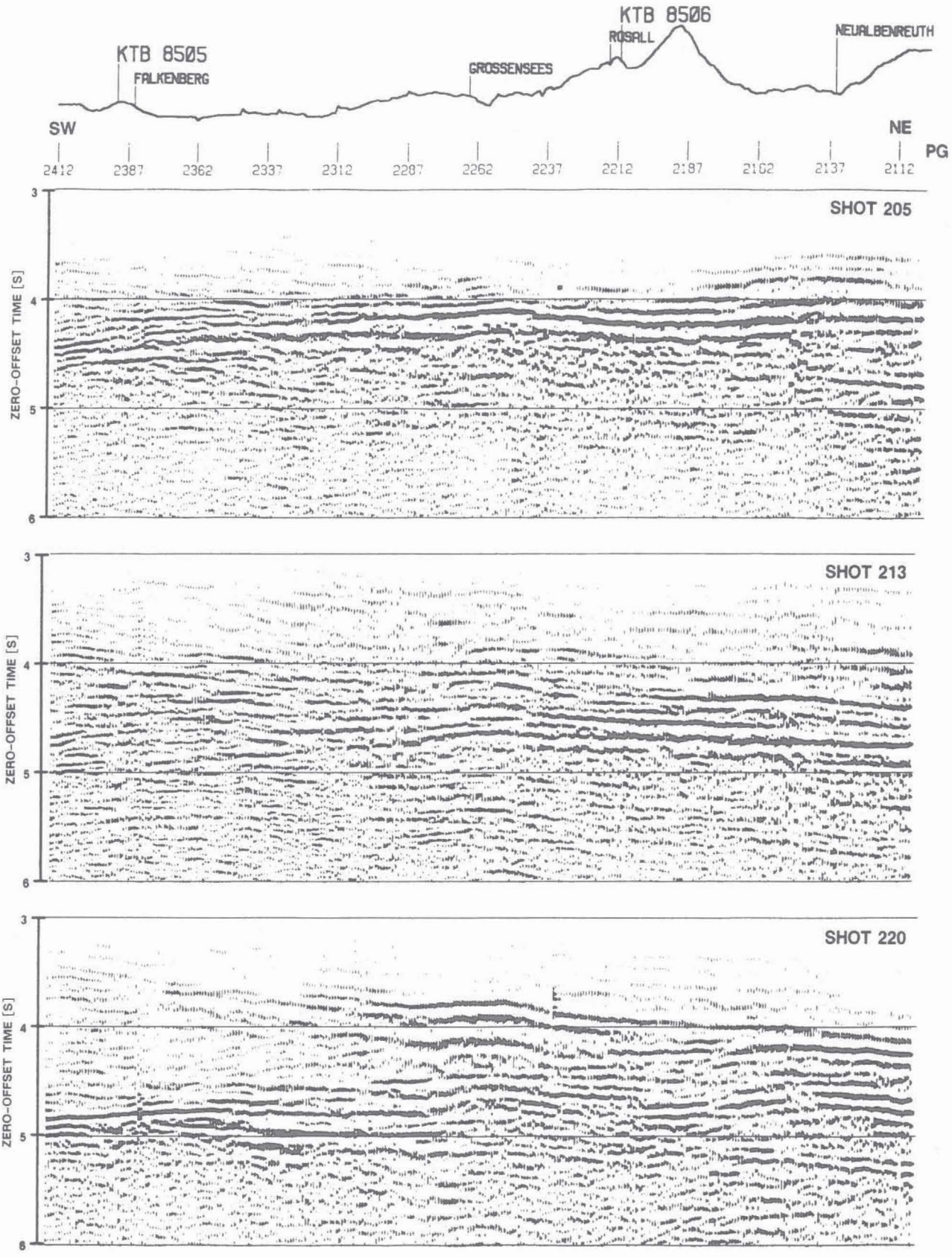

Fig.6: Simulated zero-offset sections for the same shot records as in Fig. 5 obtained by NMO-corrections with an average velocity of 5.95 km/s; P_g-onsets, being not properly transformed by NMO-corrections, have been suppressed by a ramp mute.

at PG no. 2290. Comparing the three ZOF simulations, again obtained with v_{NMO}=5.95 km/s, the dipping of the base of the EB towards SE and its bisection in the SE are clearly discernible.

Fig. 7 is an attempt to portray the NW-SE variations of the EB along the DEKORP4 line by a scenographic fence diagramm of subsections cut out from all zero-offset transformed record

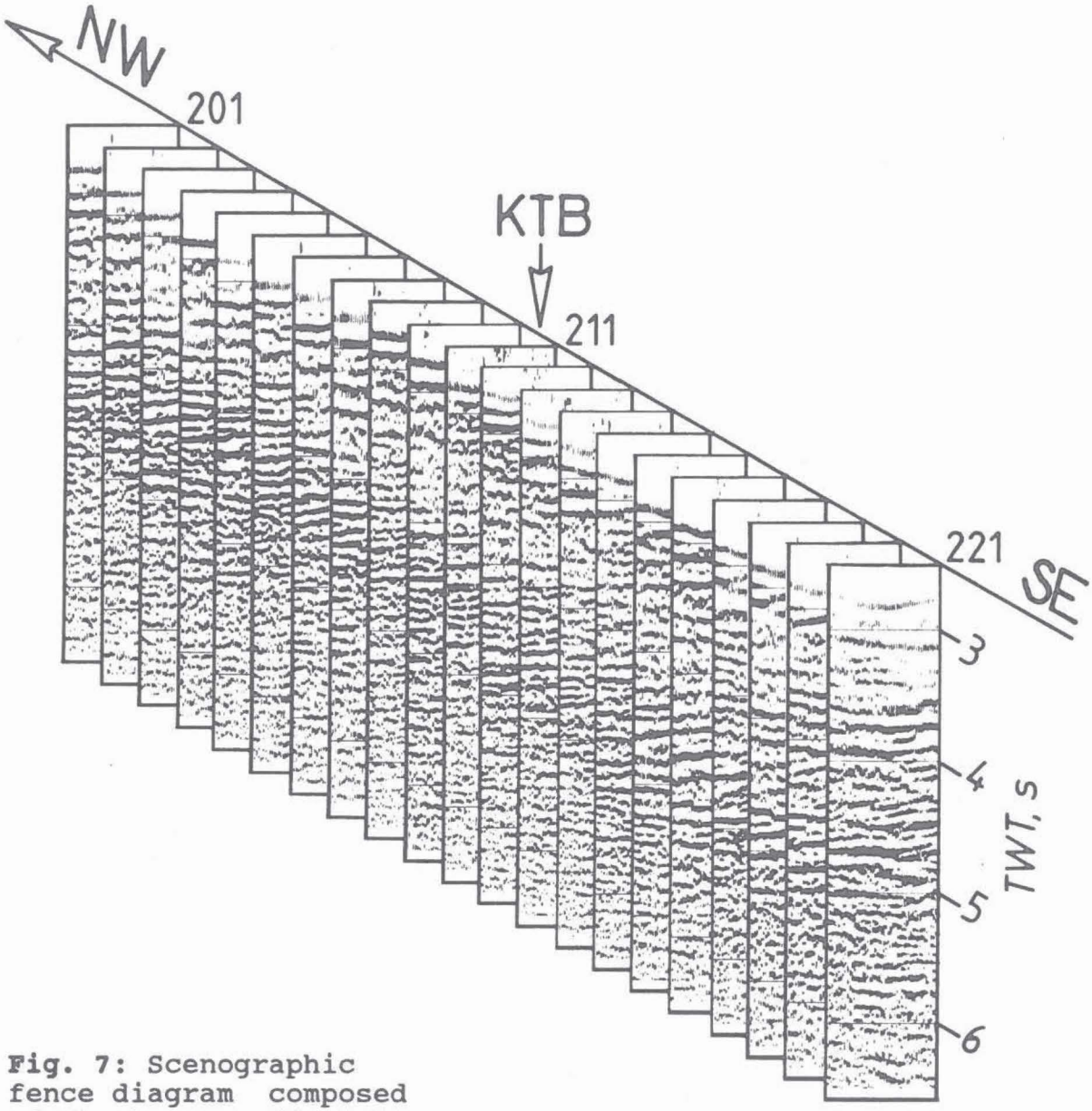

Fig. 7: Scenographic fence diagram composed of short zero-offset transformed segments (50 traces, 4 km) of ISO89 shot records 201 to 221 with midpoints beneath the DEKORP4 line and the KTB location; the NW-SE extent of the covered stripe is 10 km. Strong reflections around 4 to 5 s TWT delineate the Erbendorf-Body and its intricate internal structure. Onsets around 3 s are P_g-waves not to be considered in simulated zero-offset sections.

sections of the shot series 201 to 221. Each of the transverse subsections represents a spread of 50 channels with 80 m spacing and shot-to-receiver midpoints around the DEKORP4 line. Altogether they cover a 10 km long and 2 km broad CMP-stripe with the KTB site in the centre. The P_g-waves forming the onsets at 2.8 to 3.1 s TWT in Fig. 7 have not been muted, in contrast to Fig. 6. The typical EB reflections are present in all subsections with strong amplitudes between 4 and 5 s TWT, in the bisected SE-part they somehow rise to less than 4 s. An intricate internal structure with pronounced horizontal variations is evident, which can, however, not be resolved in de-

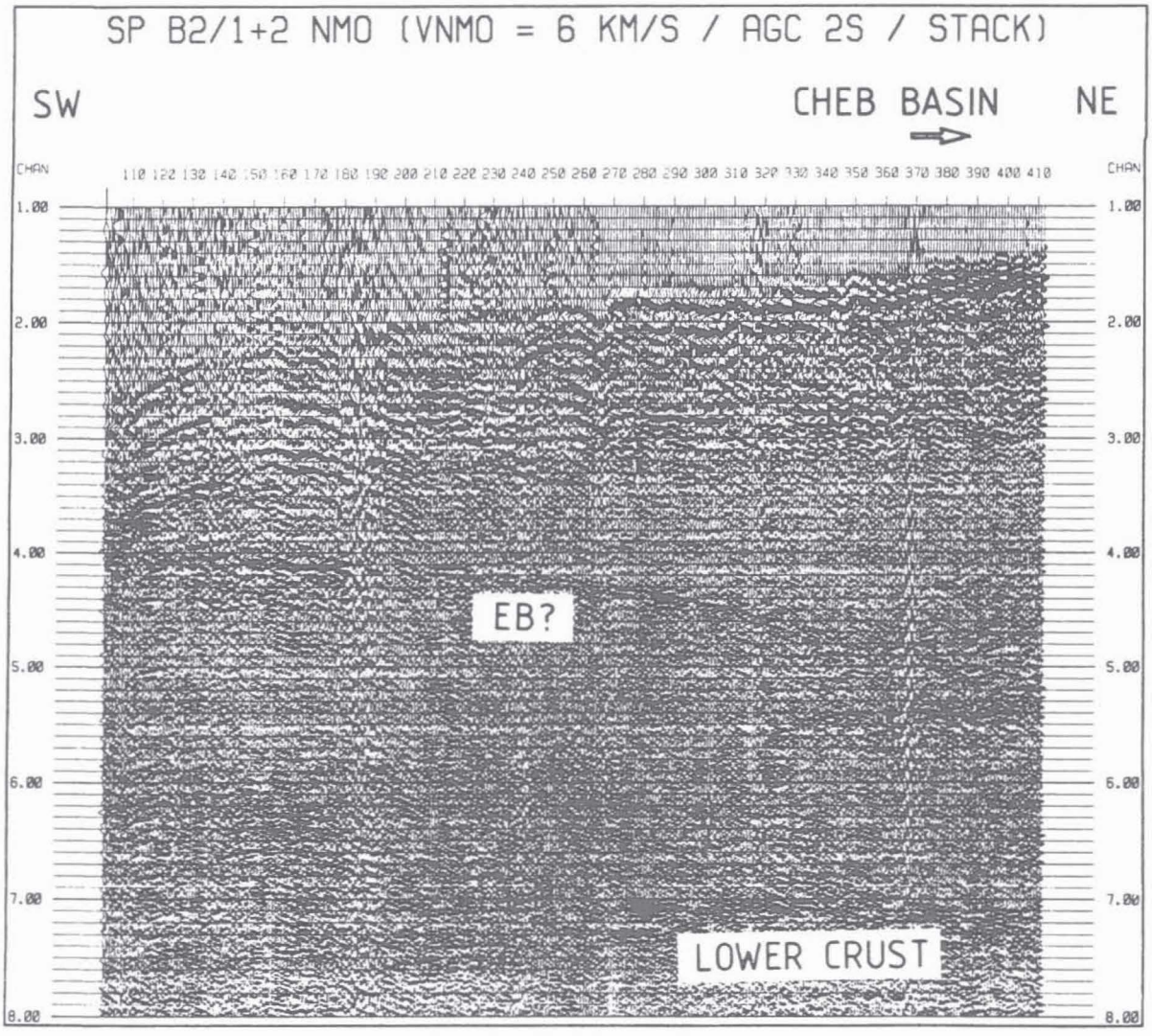

Fig. 8: Zero-offset-corrected stacked section of two shots from location B2 (CSFR) recorded along spread Reflex1. A very sharp wide-angle reflector with TWT comparable to the Erbendorf-body appears under Reflex1 and seems to dip towards the tertiary Cheb basin; a change of crustal style in that direction is indicated by the appearance of strong reflections from the top of the lower crust.

tail with the simple approach of simulated ZOF-sections. The main point to be stressed by Figs. 5 to 7 is, that the EB reflections have been observed perpendicular to the DEKORP4 line in the whole area covered from the Franconian Line to the Falkenberg granite complex with the same characteristics as earlier parallel to DEKORP4.

ISO89 has also provided evidence that the EB is not a singularity in the middle crust of the narrow KTB surroundings. Similar bodies may exist in other places of the Saxothuringian/ Moldanubian boundary zone. Fig. 8 shows a simulated ZOF-section of two stacked shots from shotpoints B2/CSFR recorded along spread Reflex1 (Fig. 3) with a very sharp wide-angle reflection of about the same TWT as the EB but with otherwise different signature. The reflector seems to dip from the SE margin of the Fichtelgebirge towards the tertiary Cheb Basin. Parallel in that a marked reflection from the top of the lower crust appears. This might indicate a tertiary regeneration of the Variscan crust at the transition to the Cheb Rift.

Simulated COF and ZOF sections are only very rough first approximations for imaging crustal structures by wide-angle reflections and should be interpreted cautiously. For a detailed and reliable imaging of strong horizontal heterogeneities the migration process is even more important in wide-angle seismics than it is in steep-angle seismics (Gebrande et al. 1989). A suitable 3D-version of the isochrone wide-angle migration method - Fig.1 is the result of a 2D-version - is presently being developed. For its hopefully successful application a comprehensive 3D velocity will be a prerequisite.

3.3 Velocity Analyses

The independent control or improvement, respectively, of the 2D velocity model derived from DEKORP4 data (DEKORP-Research Group 1988; Gebrande et al. 1989) and its extension to a 3D-model belong to the major targets of the ISO89 wide-angle survey. Seismic wave velocities are required for reliable structural imaging by steep- or wide-angle migration techniques as well as for the petrophysical, lithological and finally geodynamic interpretations.

We started velocity analysis of ISO89 data with spread Reflex2 because in this case the wide-angle data set includes observations down to zero offset, which are important for the velocity resolution in the upper crust. We used two independent methods:

- a special variant of the tau-p-inversion technique (Meichelböck 1988) and
- the so-called XTV-inversion (Gebrande et al. 1985), which is essentially a traveltime based stripping technique.

Fig. 9 shows an example for the tau-p method applied to stacked shot records 224 and 226 (Fig. 3). By means of an automatic picking algorithm manifold paths are traced through the slantstack transformed wavefield and converted to the v-z-

domain by the tau-sum method (Diebold et al. 1981). The stacked amplitudes are transferred from the tau-p into the v-z-domain and plotted as a filled-area contour-map, in which the dark crest is built up by the most coherent signals and thereby represents the dominant velocity-depth distribution half-way between shotpoint and receivers. Horizontal dark stripes marked by arrows in Fig. 9 may be due to subcritical reflections and indicate possible depths of first-order discontinuities.

The velocity-depth function picked by the geophysicist from Fig. 9 and controlled by forward modelling is shown, together with the result from the XTV-inversion of the same data, and with tau-p-inversions for shots 225/227 in Fig. 10. The tau-p-

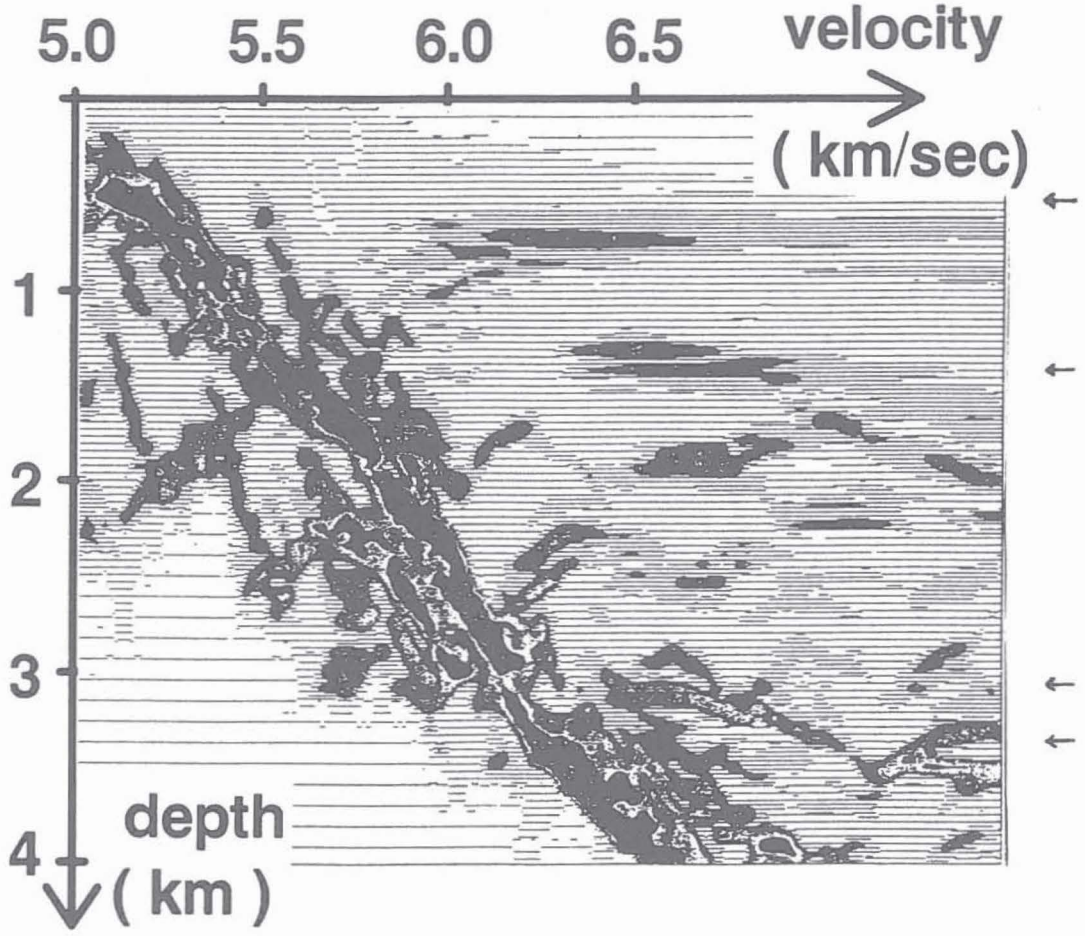

Fig. 9: Example for automatic velocity-depth determination by the modified tau-p wave-field transformation after MEICHELBÖCK (1989). The dark crest is built up by the most coherent signal amplitudes of the shot records 224 and 226 and represents the dominant velocity-depth distribution for the area of the Falkenberg granite about 10 km NE of the KTB site. Arrows mark depths of probable undercritical reflections.

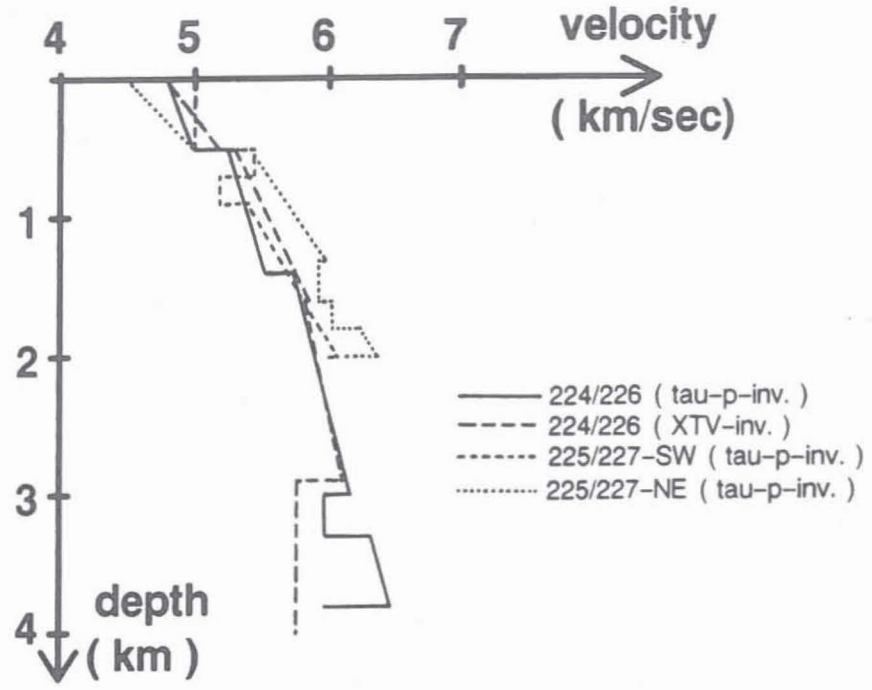

Fig. 10: Velocity-depth distributions derived by the tau-p and the XTV-method for the SW and the NE parts of line Reflex2.

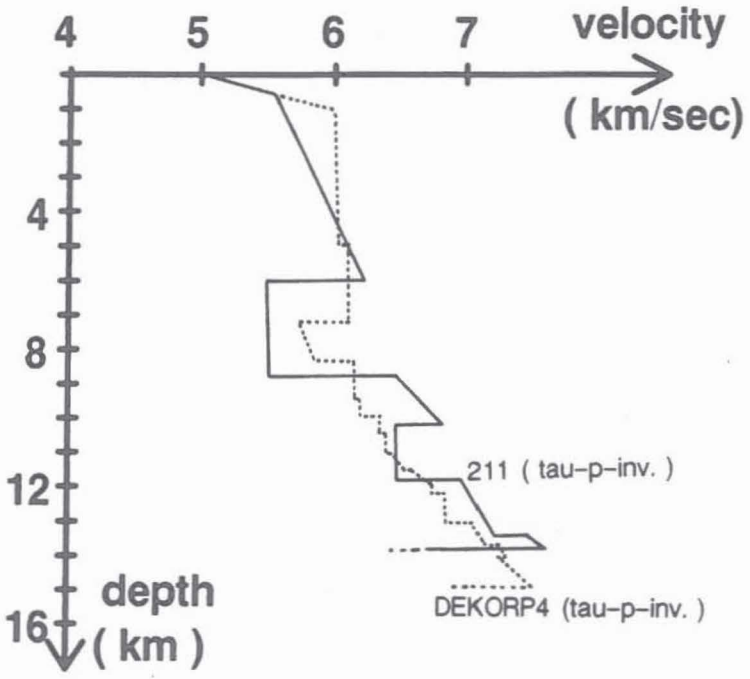

Fig. 11: Comparison of velocity-depth functions for the KTB vicinity, derived by the tau-p method from the single shot 211 recorded on line Reflex2 (SW-NE azimuth) and from CMP-sorted seismograms observed 1985 along DEKORP4 (NW-SE azimuth). The existence of p-wave velocities around 7.0 km/s at 12 to 14 km depth is corroborated by the ISO89 data. Velocity resolution in the upper 5 km is poor due to the rather large offset minimum of 25 km.

and the XTV-method provide very similar results down to a depth of about 3 km, where a low-velocity layer is expected according to both solutions. The v(z) function derived from shots 224/226 is expected to be valid for the area of the Falkenberg granite complex about 10 km NE from the KTB site.

The shots 225/227 were situated in a split-spread position in the centre of spread Reflex2 near to a boundary between granites in the SW and mica schists in the NE and have provided significantly different v(z) functions for both directions (Fig. 10). The depth of penetration is only 2 km for the split-spread data.

With regard to the EB the tau-p inversion of the shot 211, recorded on spread Reflex2 is of special interest, because the corresponding midpoints, to which the results of one-dimensional velocity determinations should be attributed, cross the KTB site (Fig. 11). The results are limited by missing observations in the 0 to 25 km offset range but, nevertheless, the v(z) function seems to be well constrained at depths greater 5 km by clear first and later arrivals recorded on spread Reflex2. Allowance for sediments beneath the shotpoint was made by a static correction of 300 ms prior to the slantstack. P-wave velocities around 7.0 km/s in 12 to 14 km depth corroborate former results from the DEKORP4 line and confirm that they are not an artifact by some strange side-effect. The unusual high wave velocities as well as the high wide-angle reflectivity of the Erbendorf-Body seem to be regional phenomena of the Earth's crust in the surroundings of KTB. The pronounced low-velocity zone obtained for the shot 211 is a surprise and needs further verification.

3.4 Polarization Analysis and Shear-Wave-Splitting

The operation of 3-component geophones recording nearly all seismic sources of the ISO89 project in the KTB pilot hole offered the unique possibility to analyze traveltime and wavefields of the wide-angle shots at depth. In view of convincing evidence for ultrasonic p- and s-wave anisotropy in almost all core samples from the KTB pilot hole (Lippmann et al. 1989; Zang et al. 1989) the question of large scale seismic in-situ anisotropy in the KTB surroundings calls for an answer. It's a question of fundamental interest going well together with the KTB project, but also a question of great practical importance, because significant anisotropy would require serious modifications in seismic processing.

The down-hole recordings from the first week of the ISO89 wide-angle measurements with shotpoints 101 to 120 are especially appropriate for an exploration of anisotropy effects because 4 (of 5) 3-component geophones were in perfect operation at that time. Details of geophone positions and orientation of components are given in Table 2.

As a first step we testet our two-dimensional isotropic velocity model derived from DEKORP4 wide-angle data against the

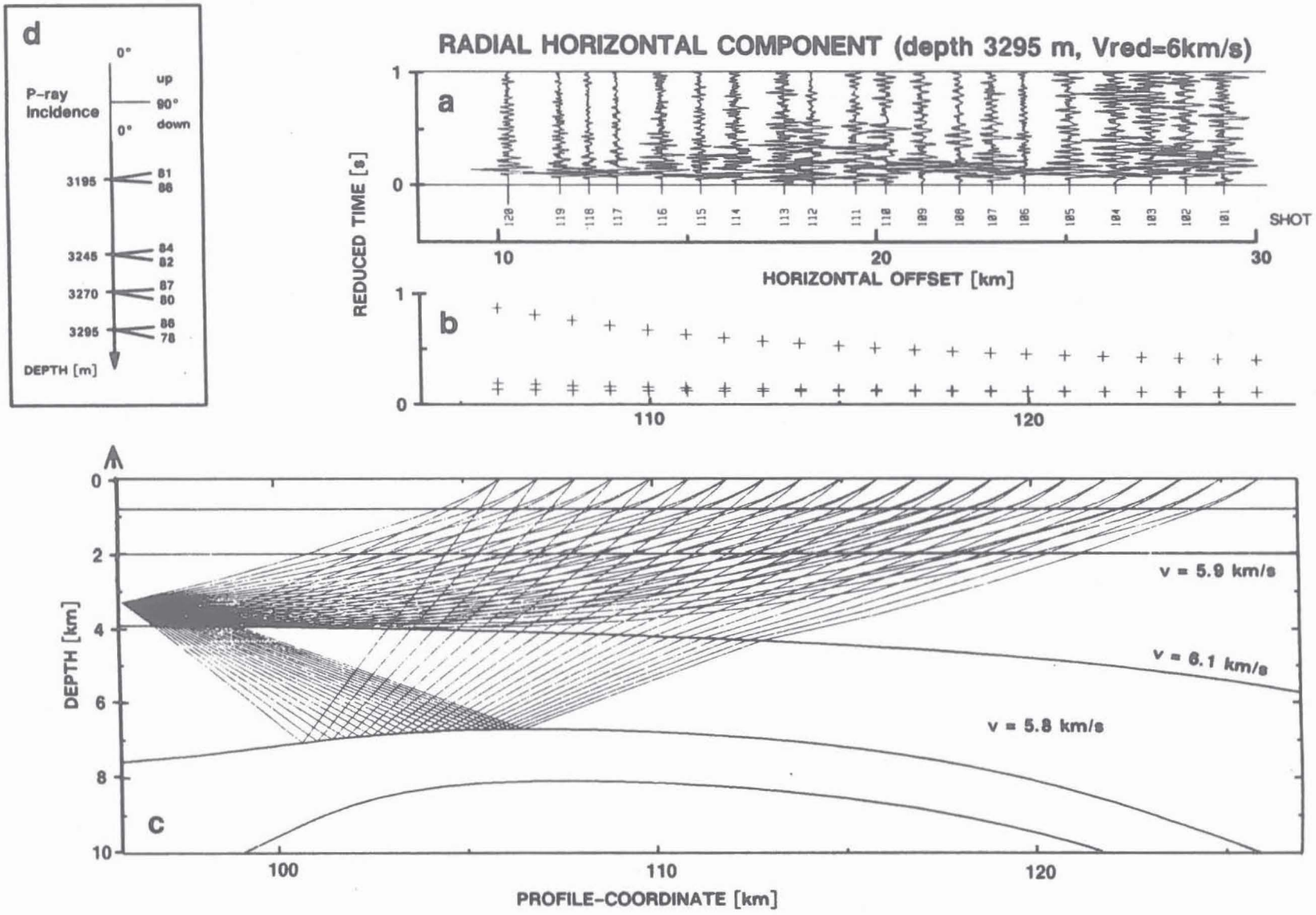

Fig. 12: Comparison of observed (a,d) and predicted (b,c) traveltimes and angles of incidence for 3-component down-hole measurements at 3295 m depth

ISO89 down-hole observations. Fig. 12a and b show the p-wave record-section in reduced time for the shot series 101 to 120 recorded by the geophone at 3295 m depth (a) in comparison with traveltimes (b) predicted from the model (c). The observed arrival times are about 0.1 s faster than predicted, but the average apparent velocities coincide rather well. The more or less horizontal incidence of the seismic rays predicted by the model calculations fits in with the results of polarization analyses of the 3-component recordings, which were performed by calculating the direction of the principal axis with the largest eigenvalue of the covariance matrix (Kanasevich, 1973).

Surprisingly the azimuth of the p-wave polarization proved to be in close agreement with the shot-to-receiver azimuth (Table 2). This means that either there is no significant p-wave anisotropy or the azimuth of wave propagation, i.e. the SE-NW direction, is close to a specific direction of pure longitudinal polarization in an anisotropic upper crust. Larger differences between p-wave polarization and propagation directions for other shotpoints, e.g. for quarries NNE from the KTB site, are in favour of the second explanation, and this becomes indeed evident by the investigation of shear-waves. In Fig. 13

Table 2: Receiver positions of the 3-component borehole geophone chain and orientation of its horizontal components according to compass readouts and p-wave polarization directions (assuming longitudinal particle motion)

sensor location number	depth [m]	component code	component type	horizontal receiver-azimuth [N°E] from compass readout	horizontal receiver-azimuth [N°E] from polarisation analysis
		111	vert.	---	---
1	3195	233	horz. H1	52	59 +/- 5
		333	horz. H2	142	149 +/- 5
		111	vert.		
2	3220	233	horz. H1		
		333	horz. H2	defectiv component H2	
		111	vert.	---	---
3	3245	233	horz. H1	19	26 +/- 4
		333	horz. H2	109	116 +/- 4
		111	vert.	---	---
4	3270	233	horz. H1	24	24 +/- 2
		333	horz. H2	114	114 +/- 2
		111	vert.	---	---
5	3295	233	horz. H1	248	249 +/- 4
		333	horz. H2	338	339 +/- 4

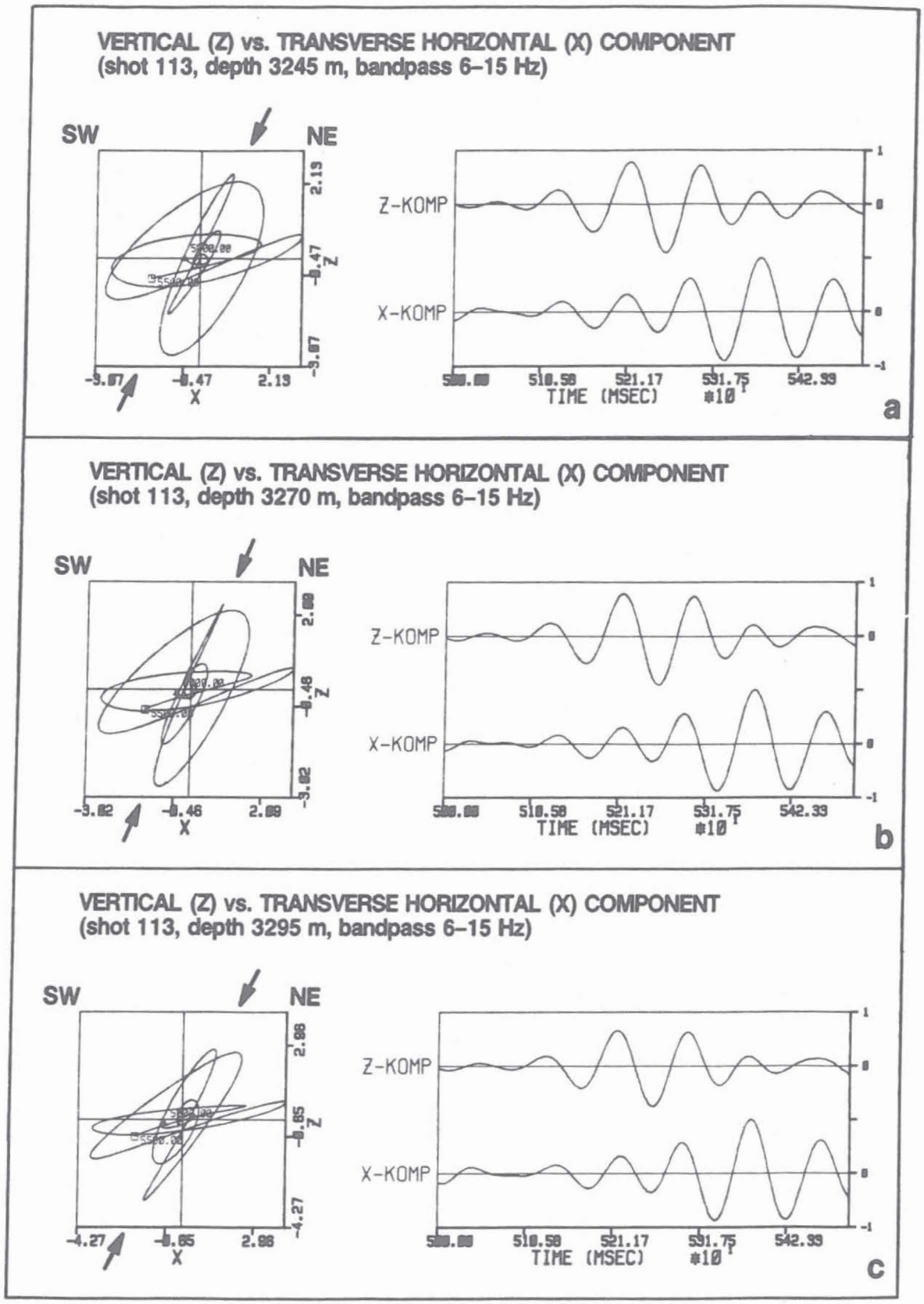

Fig. 13: S-wave components and s-wave hodographs showing s-wave splitting

typical s-wave signals of a shot (no. 113) recorded in three different depth positions are plotted in the vertical plane normal to wave propagation and p-wave polarization. The components as well as the hodographs are displayed providing clear evidence for birefringence (shear-wave splitting). The s-wave trains start consistently with linear polarization dipping steeply (65 degree) to the SW and continue with more elliptical particle motion, which seems to be due to a superimposed orthogonally polarized shear-wave with slower propagation velocity. All records exhibit this general behaviour.

Decomposition of the 3-component seismograms into mutually orthogonal components parallel and normal to the p-wave polarization direction provides an almost perfect separation of p- and s-waves as demonstrated by Fig. 14a. By an appropriate additional rotation of the transverse components in the normal plane also the fast and the slow shear-waves can be separated. This is shown in Fig 14b for the four records of shotpoint no. 113. It becomes evident that the delay of the slow shear-wave is more than one period (about 100 ms) and this is also true for most of the other shot and receiver positions. This delay cannot be the result of a very local anisotropy, e.g. merely at the source or receiver. With a reasonable anisotropy coefficient of 5 to 10%, the waves must propagate through at least several km of anisotropic rocks to bring forth the observed delay.

Fig. 15 shows record sections of the decomposed fast and slow shear-waves for the total shot series recorded at 3295 m depth. Shear-wave splitting is evident, but there is no linear increase of delay-times with shot-to-receiver distances, as would be expected for a medium with constant anisotropy. Fluctuations seem to be of a scale of about 10 km; at the scale of seismic field experiments, however, they are not simply averaged out.

From comparison with laboratory investigations on KTB core samples and from theoretical considerations it is expected that rock foliation is the main cause for the observed anisotropy and that the polarization direction of the fast s-wave is in the plane of foliation. This would imply that the dipping polarization of the fast shear-wave reflects the dominant inclination of foliation in the zone of Erbendorf-Vohenstrauß SE of the KTB location. Shear-wave polarization is worth to be studied. With consequent methodical development it might become a diagnostic tool for the seismologist as useful as the polarization microscope is for the petrologist.

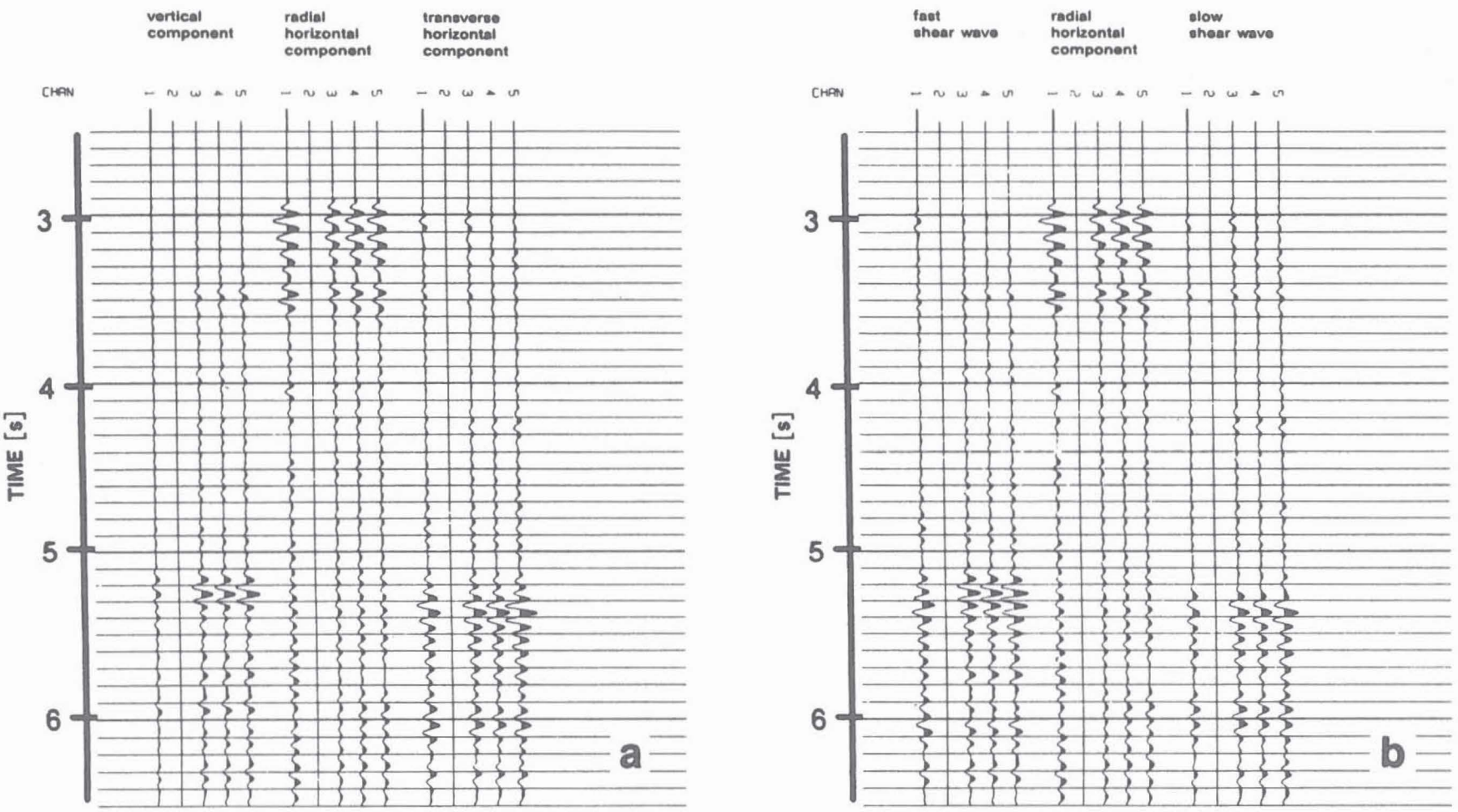

Fig. 14: Decomposition of four 3-component seismograms in (a) p- and s-waves and (b) p-, fast s- and slow s-waves by appropriate rotations

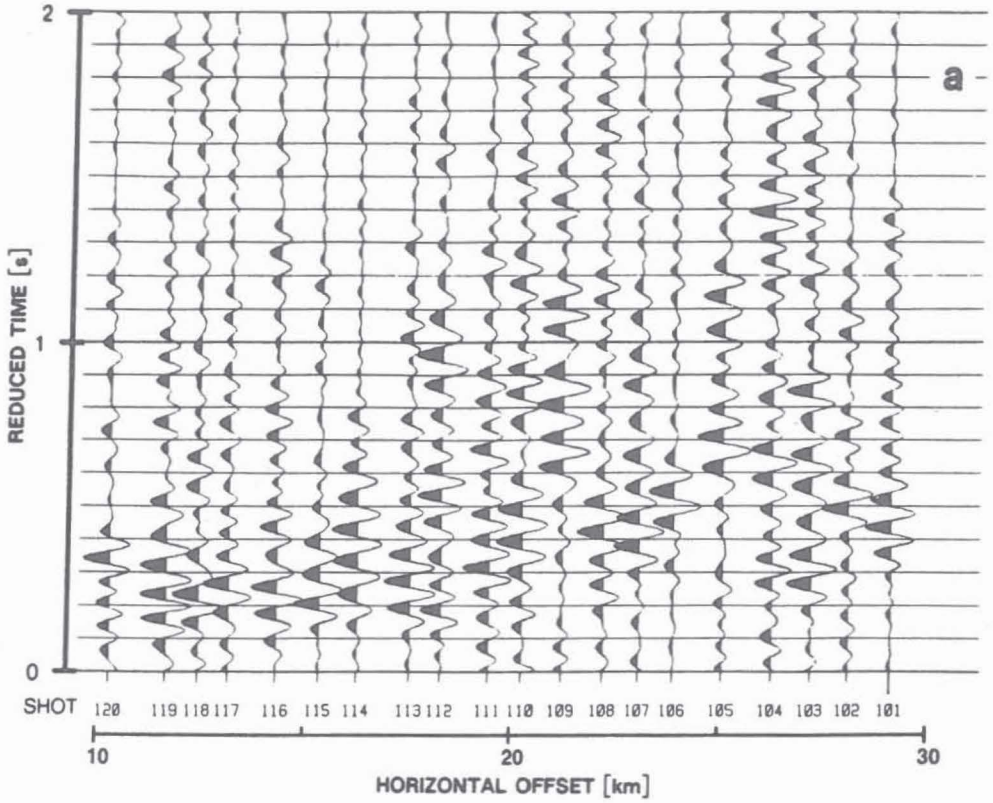

FAST SHEAR WAVE (depth 3295 m, bandpass 6–15Hz, Vred=3.5km/s)

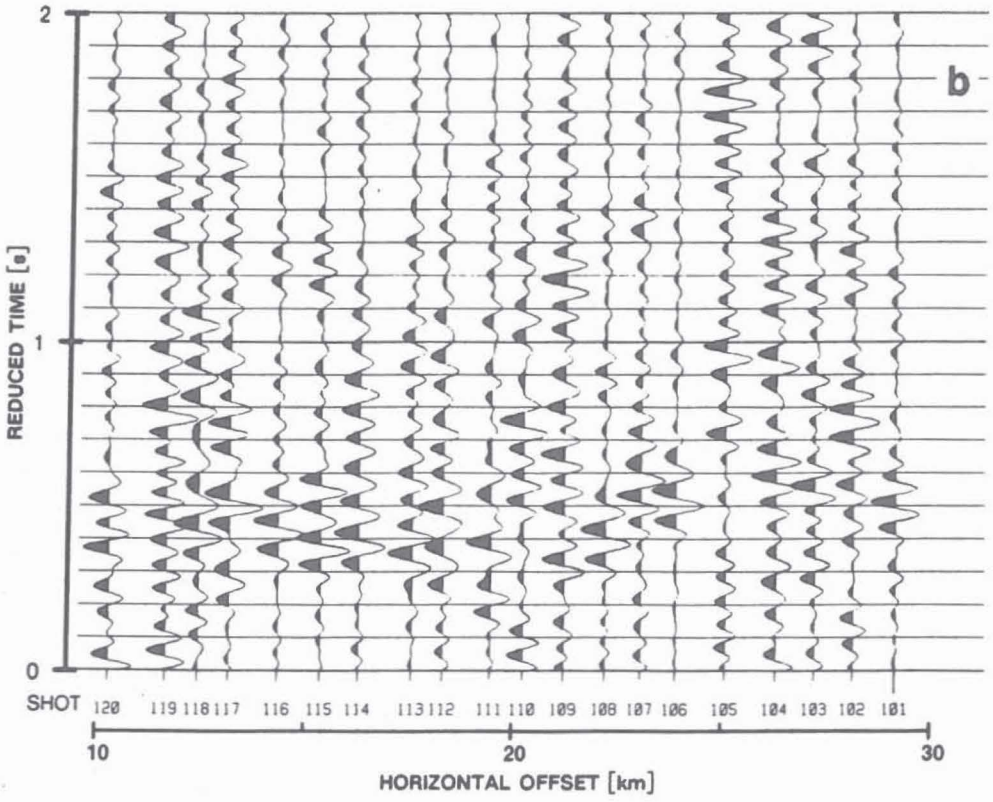

SLOW SHEAR WAVE (depth 3295 m, bandpass 6–15Hz, Vred=3.5km/s)

Fig. 15: Comparison of the separated fast (a) and slow (b) shear-waves for all shotpoints recorded in 3295 m depth; shear-wave splitting is beyond all doubt.

Acknowledgments. The funding of the investigations by the Federal Ministry of Science and Technology (BMFT), Bonn, is gratefully acknowledged. We appreciate the continuous support by the DEKORP steering committee and by H. Soffel, director of the Institut für Allgemeine und Angewandte Geophysik, München. Thanks for excellent cooperation during field work are due to the teams from the Geophysical Institutes of Aachen, Clausthal, Karlsruhe, Münster, Zürich and München, from the Geological Survey of Lower Saxony, the Prakla-Seismos crew and to the collegues from Geofyzika Brno.

References

DEKORP Research Group: Results of the DEKORP4-KTB Oberpfalz deep seismic reflection investigations. J.Geophys. 62, 69-101, 1988

Diebold, J.B., Stoffa, P.L.: The traveltime equation, tau-p mapping and inversion of common midpoint data. Geophysics 46, 238-254, 1981

Gebrande, H., Miller H.: Refraktionsseismik. In: Angewandte Geowissenschaften - Band II, Bender, F., ed.: 226-260. Stuttgart: F. Enke Verlag, 1985

Gebrande, H., Bopp, M., Neurieder, P. and Schmidt, T.: Crustal Structure in the Surroundings of the KTB Drill Site as derived from Refraction and Wide-Angle Seismic Observations. In: The German Continental Deep Drilling Program (KTB), R. Emmermann and J. Wohlenberg eds.: 151-176, Springer-Verlag, 1989

Giese, P.: Versuch einer Gliederung der Erdkruste im nördlichen Alpenvorland, in den Ostalpen und in Teilen der Westalpen mit Hilfe charakteristischer Refraktions-Laufzeit-Kurven sowie eine geologische Deutung. Geophysikalische Abhandlungen 1(2), 202 p., Freie Universität Berlin. Berlin: Friedrich Reimer Verlag, 1968

Giese, P.: Results of data generalization. In: Explosion seismology in Central Europe, Giese, P., Prodehl, C., Stein, A., eds.: 339-346. Berlin: Springer Verlag, 1976

Kanasewich, E.R.: Time Sequence Analysis in Geophysics. University of Alberta Press, 1973

Lippmann, E., Bücker, C., Huenges, E., Rauen, A., Wolter, K., Soffel, H.C.: Rock physical properties: first results of the KTB-field-labratory. Scientific Drilling 1, 143-149, 1989

Meichelböck, M.: Tau-P-Inversion, - mit Anwendungen auf DEKORP4-Weitwinkel- und Refraktionsmessungen. Dipl.-Arbeit, Inst. f. Allg. u. Angew. Geophysik der Ludwig-Maximilians-Universität München, 1988

Peters, K.: Ergebnisse der Gravimetrie im Bereich der Münchberger Gneismasse und der Refraktionsseismik längs eines Profils über die Gneismasse. Diss. Ludwig-Maximilians-Universität München, 131 p., 1974

Schmidt, T.: Seismisches Abbilden durch Isochronen-Migration von Weitwinkeldaten am Beispiel des DEKORP4-Profils. Diss. Ludwig-Maximilians-Universität, in Vorbereitung, 1988

Schmoll, J., Bittner, R., Dürbaum, J., Heinrichs, T., Meißner, R., Reichert, C., Rühl, T., Wiederhold: Oberpfalz Deep Seismic Reflection Survey and Velocity Studies. In: Exploration of the Continental Crust through Drilling IV, Emmermann, R., Wohlenberg, J., eds. Berlin: Springer Verlag, 1988

Seidl, D.: The Simulation Problem for Broad-Band Seismograms. J. Geophys. **48**, 84-93, 1980

Zang, A., Wolter, K., Berckhemer, H.: Strain recovery, microcracks and elastic anisotropy of drill cores from KTB deep well. Scientific Drilling **1**, 115-126, 1989